We are IntechOpen, the world's leading publisher of Open Access books Built by scientists, for scientists

6,900
Open access books available

186,000
International authors and editors

200M
Downloads

Our authors are among the

154
Countries delivered to

TOP 1%
most cited scientists

12.2%
Contributors from top 500 universities

WEB OF SCIENCE™

Selection of our books indexed in the Book Citation Index in Web of Science™ Core Collection (BKCI)

Interested in publishing with us?
Contact book.department@intechopen.com

Numbers displayed above are based on latest data collected.
For more information visit www.intechopen.com

8

Shape Measurement of Solar Collectors by Null Screens

Víctor Iván Moreno-Oliva,[1] Rufino Díaz-Uribe[2] and Manuel Campos-García[2]
[1]*Universidad del Istmo (UNISTMO), Campus Tehuantepec, Oaxaca,*
[2]*Universidad Nacional Autónoma de México, CCADET-UNAM, México, D.F.*
México

1. Introduction

The optical performance of solar concentrating collectors is very sensitive to inaccuracies of components and assembly. Because of the finite size of the sun and errors of the collector system (e.g., tracking, receiver alignment, mirror alignment, mirror shape, and mirror specularity) the intensity of light at the focal receiver is reduced.

Among the principal methods for testing optical surfaces, the Ronchi and Hartmann tests have been popular for many years for testing slow (F/# >> 1) spherical and aspherical surfaces (Cornejo-Rodríguez, 2007; Malacara-Doblado & Ghozeil, 2007). Both methods for testing optical system are useful mainly for surfaces of revolution. Previous works (Shortis & Johnston, 1996; Pottler & Lüpfert, 2005) have described the application of photogrammetry to the characterization of solar collectors. Briefly, close-range photogrammetry involves the use of a network of multiple photographs of a target objet (a solar collector component in this case) taken from a range of viewing positions, to obtain high-accuracy, 3D coordinate data of the object being measured. Furthermore, photogrammetry is self contained and requires little external information if only the shape and size of the object is of interest.

Other works propose a system called Scanning Hartmann Optical Test (SHOT), and Video Scanning Hartmann Optical Test (VSHOT), in these methods a mirror is typically positioned at a distance slightly greater or less than twice its focal length (f). Then a laser beam is steered by a 2-axis scanner to a point on the mirror. After reflecting off the mirror, the laser beam returns to a location near its source and reaches a CCD camera. A computer video board digitizes the CCD camera's image and the centroid location of the reflected spot is calculated. The laser is scanned quickly across the surface of the mirror and this process is repeated many times. The concentrator's slope at each point of reflection and a polynomial surface fit to the measured slopes is then calculated. The accuracy of the VSHOT device depends upon the geometry of the test setup (F#, distance, laser spot size, etc.) and the accuracy of input data (distance, scanner calibration, video calibration, etc.).

On the other hand, the null screen method consists of a screen with an array of points or lines that by reflection on an ideal surface, gives a perfect square array of points or lines at a CCD camera, while any departure of the ideal geometry is indicative of shape errors of the surface. The shape can be obtained through the general and exact formula proposed by (Díaz-Uribe, 2000).

In this Chapter we describe the principles of the null screen method and show the implementation for concave (Campos-García et al., 2008) and convex (Díaz-Uribe & Campos-García, 2000) surfaces and also some new developments in the null screen method (section 2). The application of the null screen principles to the testing of solar collector components (parabolic trough solar collector PTSC (section 3) and parabolic dish solar collector systems (section 4)) are described.

2. Null screen principles (testing fast convex and concave surfaces)

The null screen method has been successfully used in testing optical surfaces of revolution, both concave and convex, of small and medium size. The method is regarded as an extension of the Hartmann test. The Hartmann test (Malacara-Doblado & Ghozeil, 2007) uses a perforated screen for sampling the wave front when the surface is illuminated by a point source; by reflection on the mirror, the light passing through the holes gives a set of bright spots on a plane screen parallel to the perforated screen, close to the point source (or its conjugated plane). The positions of the bright spots give the derivative of the wave front at each point of incidence on the mirror. The essential principle of the null screen method is to design screens, when you know the ideal shape of the surface under test. The null screen contain an array of curves or spots such that, when the screen is observed by reflection on the real surface, the image in the optical system consists of an array of perfectly square straight lines or bright spots if the test surface is perfect; if the surface is of high optical quality the distortion of the lines is null (hence the null term in the name). Otherwise, if the image of the array is not square, the deformations are due to imperfections, defocus or misalignment of the test surface. With this technique the alignment of the optical system is relatively easy.

To test a surface of revolution, the points of the designed null screen are plotted on a sheet of paper with the help of a laser printer (or a plotter, depending on the size of the screen); then, the paper is rolled into a cylindrical shape and inserted into a transparent acrylic cylinder which supports the paper. In the test of concave surfaces the diameter of the cylindrical screen must be many times smaller than the diameter of the surface under test (Fig. 1a), and for convex surface the diameter of the test surface defines the minimum diameter used for the cylindrical screen, in this case the test surface lies inside the cylindrical screen (Fig. 1b). Figure 1 also shows the inverse trace of a ray starting from a point P_1 of the image plane (CCD plane) passing through the small aperture lens stop (point P). This ray reaches the test surface at the point P_2 and, after reflection, the ray hits the cylindrical screen at P_3. The distances a and b are the CCD-pinhole distance and the distance between the pinhole and the vertex of the surface respectively; they are related by

$$b = \frac{aD}{d} \pm \beta\,, \tag{1}$$

where D is the diameter of the test surface, d is the length of the smallest side of the CCD and β is the sagitta at the rim of the surface. The plus sign refers to concave surface and the minus to convex surface, and which for a conical surface is given by

$$\beta = \begin{cases} \dfrac{D^2}{8r} & \text{for } k = -1 \\ \dfrac{r}{k+1}\left\{1 - \left[1 - \dfrac{(k+1)D^2}{4r^2}\right]^{1/2}\right\} & \text{for } k \neq -1. \end{cases} \tag{2}$$

where k is the conic constant of the test surface.

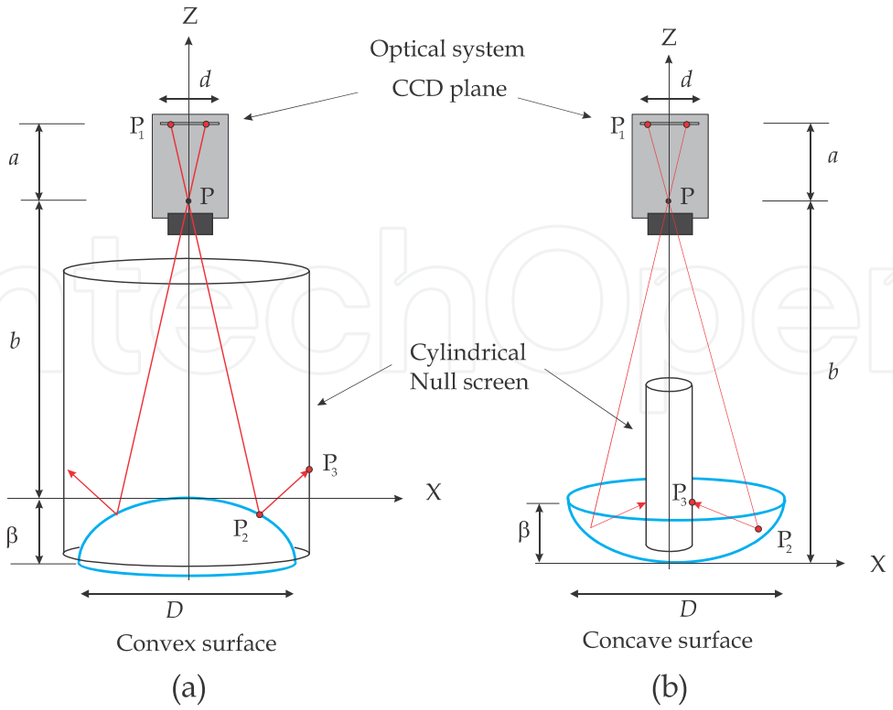

Fig. 1. Setup for testing a) a convex and b) a concave

2.1 Practical implementation of the screen

As a proof of principle, we show a qualitative test on two surfaces. The first is a concave hyperbolic surface, and the second is a convex spherical surface.

2.1.1 Hyperbolic concave surface

The concave hyperbolic surface used was built as a mold for casting the secondary convex mirror of an infrared telescope; the surface was 459 mm in diameter (F/0.5087). The screen was designed with the values given in Table 1. Figure 2b shows the actual null screen before being wrapped around an acrylic cylinder; the units are in millimeters.

Element	Symbol	Size
Surface radii of curvature	r	467 mm
Conic constant	k	-1.345
Surface diameter	D	459 mm
Camera lens focal length	a	12 mm
CCD length	d	6.6 mm
Stop aperture-surface vertex	b	889.81 mm

Table 1. Design parameters for the test of the hyperbolic surface.

Figure 2a shows the null screen wrapped around the acrylic cylinder and the hyperbolic test surface; finally, Figure 2c shows the resultant image of this screen after reflection on the test surface. It is clear that at the center of the surface, the image is almost a perfect square array of grid lines; going to the edge of the surface, the grid lines are deformed depending on the slope of the surface.

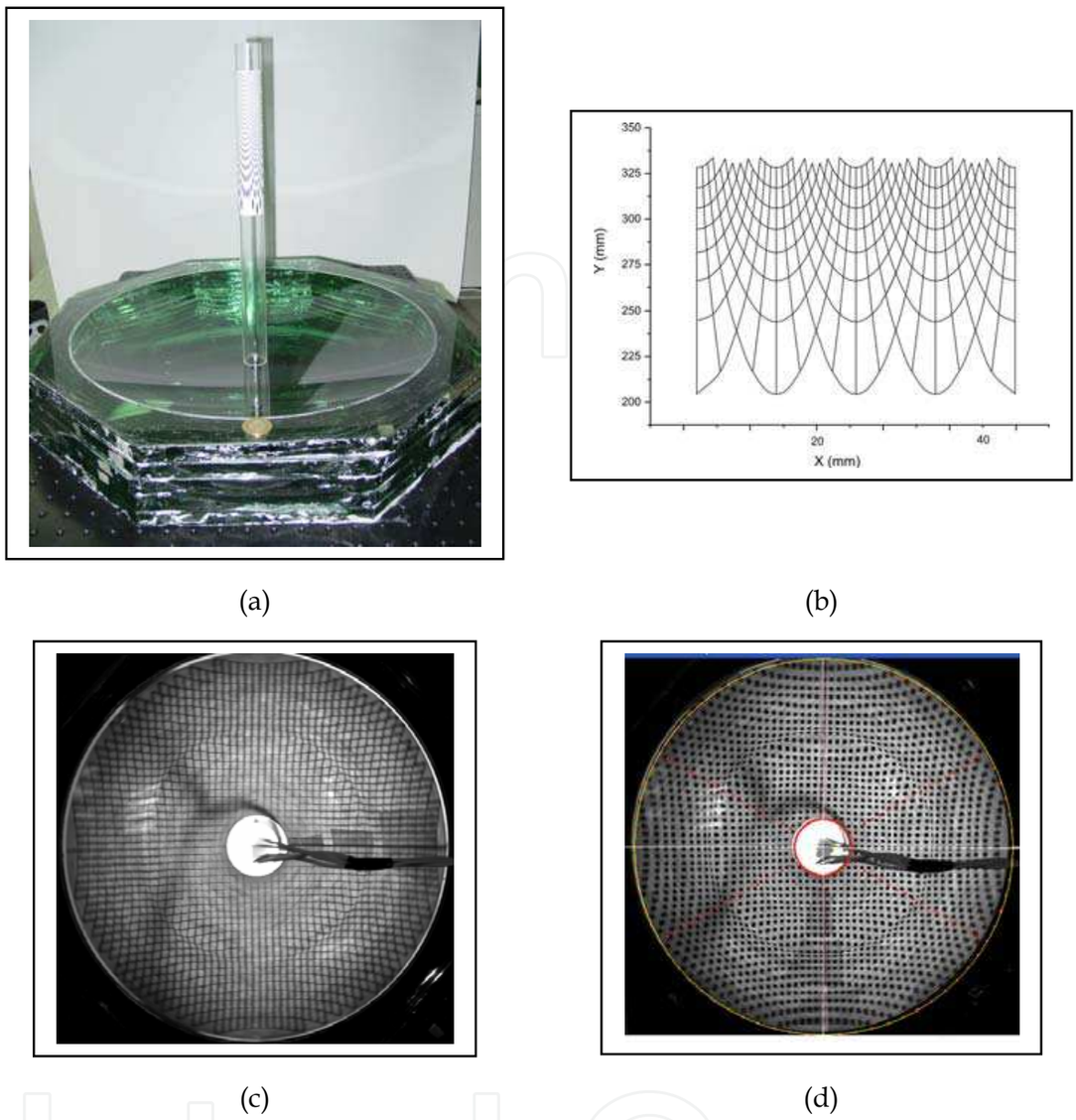

Fig. 2. a) The hyperbolic surface with the null screen, b) Flat printed null screen with grid lines for qualitative testing, c) resultant image of the screen shown in (b) reflection on the test surface and d) resultant image by a null screen with drop shaped spots for quantitative testing.

For a quantitative testing of the surface, a null screen with drop-shaped spots is used (Fig. 2d) to simplify the measurement of the positions of the spots on the CCD plane, which are estimated by the centroids of the spots on the image of the null screen.

2.1.2 Spherical convex surface

The spherical convex surface used was a steel ball with a diameter of 40 mm; the proposed cylindrical null screen was 60 mm in diameter. For a qualitative evaluation of the shape of the surface, we designed a screen to produce a square array of 19x19 lines on the image plane. Figure 3a shows the spherical surface, in Fig. 3b the flat printed null screen is shown, and the image of the cylindrical screen after reflection on the spherical surface is shown in

Fig. 3c; the image is almost a perfect square grid but, in this case, the departures from a square grid which can be seen are probably due to a defocus of the surface and some printing errors, and not to deformations of the surface.

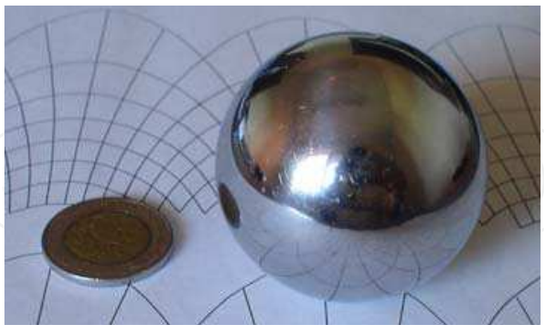

(a)

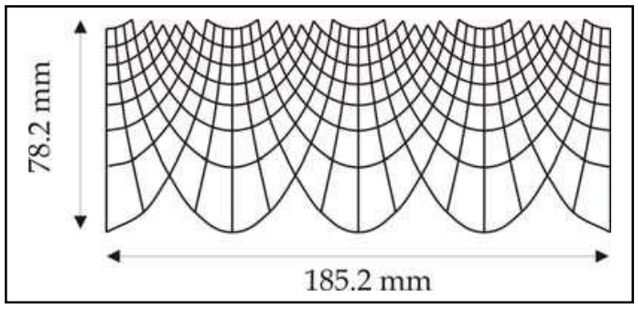

(b) (c)

Fig. 3. a) Spherical surface (steel ball), b) flat printed null screen with grid lines for qualitative testing, and c) the resultant image of the screen after reflection on the test surface.

2.2 Surface shape evaluation

The shape of the test surface can be obtained from measurements of the positions of the centroids of the spot images on the CCD plane through the formula (Díaz-Uribe, 2000)

$$z - z_0 = \int_{P_o}^{P} \left(\frac{n_x}{n_z} dx + \frac{n_y}{n_z} dy \right), \tag{3}$$

where n_x, n_y, and n_z are the Cartesian components of the normal vector **N** on the test surface, and z_0 is the sagitta for one point of the surface. The value of z_0 is not obtained from the test, but it is only a constant value that can be ignored.

The evaluation of the normals to the surface consists of finding the directions of the rays that join the actual positions P_1 of the centroids of the spots on the CCD and the corresponding Cartesian coordinates of the objects of the null screen P_3. According to the reflection law, the normal **N** to the surface can be evaluated as

$$\mathbf{N} = \frac{\mathbf{r}_r - \mathbf{r}_i}{\left|\mathbf{r}_r - \mathbf{r}_i\right|}, \tag{4}$$

Where $\mathbf{r}_i$ and $\mathbf{r}_r$ are the directions of the incident and the reflected rays on the surface, respectively; the reflected ray passes through the pinhole P and arrives at the CCD image plane at P_1 (Fig. 4). For the incident ray $\mathbf{r}_i$ we only know the point P_3 at the null screen, so we have to approximate a second point to obtain the direction of the incident ray by intersecting the reflected ray with a reference surface; the reference surface can be the ideal design surface or a similar surface close to the real one.

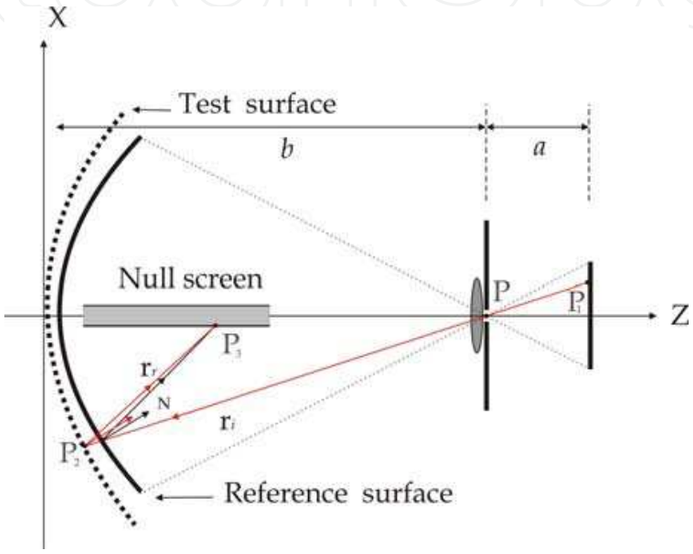

Fig. 4. Approximated normals.

The next step is the numerical evaluation of Eq. (3). The simplest method used for the evaluation of the numerical integration is the trapezoid rule (Malacara-Doblado & Ghozeil, 2007). An important problem in the test with a null screen is that the integration method accumulates important numerical errors along the different selected integration paths. It is well known (Moreno-Oliva et al., 2008a) that a bound to the so called truncation error can be written as

$$|\varepsilon| \le \frac{h^2}{12}(b-a)M, \tag{5}$$

here h is the maximum separation of two points along the integration path, (b-a) is the total length of the path and M is the maximum value of the second derivative of the integrand along the path. Díaz-Uribe et al. (2009) have shown that for spheres this error is negligible; for other surfaces it can be very significant.

To reduce the numerical error, some authors have proposed the use of parabolic arcs instead of trapeziums (Campos-García et al., 2004), or the fit of a third degree polynomial that describes the shape of the test surface locally(Campos-García & Díaz-Uribe, 2008).

There are other integration methods going from local low order polynomial approximations (Salas-Peimbert et al., 2005) to global high order polynomial fitting to the test surface (Mahajan, 2007) in the latter case, the Least Squares method is commonly used but some

other fitting procedures, such as Genetic Algorithms (Cordero-Dávila, 2010) or Neural Networks, have been also used.

By far the simplest integration method is the trapezoid rule method; however, since the error increases as the second power of the spacing between the spots of the integration path, to minimize the error, it is desirable to reduce the spacing between spots (see eq. (5)). This implies more spots in the design of the null screen; there is, however, a physical limit on the number of spots; if the spot density is too large,the spot images can overlap because of defocus, aberrations or because of diffraction. A method to increase the number of points, thus reducing the average separation between them, is to use the so called point shifting method (Moreno-Oliva et al., 2008a; Moreno-Oliva et al., 2008b). The basic idea is to acquire a total of m pictures, each with different null screen arrangement and containing n spots on the image; the spots will be shifted from their positions in other pictures, making a total of $m \times n$ evaluation points, with an average separation of

$$h_m = \frac{h}{\sqrt{m}}. \tag{6}$$

Then, the bound to the truncation error is reduced as the original bound for only one image (n points), divided by m

$$|\varepsilon_m| \leq \frac{h^2}{12m}(b-a)M \leq \frac{|\varepsilon|}{m}. \tag{7}$$

In order to implement this method in the lab, small known movements are applied to the cylindical screen along the axis of the surface under test. With this method it was possible to reduce the accumulated numerical error by up to 80%, with respect to the error for a single screen without scrolling. In Fig. 5a the image for the initial position of the screen is show; and figure 5b is the image for the final position of the screen. A total of ten images were captured. Each image was independently captured and processed to obtain the centroids of the spots, Fig. 5c shows the plot of the spot centroids for all the captured images.

Another method to implement the same idea is to design a screen such that its image in the optical system is an array of dots or spots in a spiral arrangement (Moreno-Oliva et al., 2008b). In this case the movement of the screen or surface is made by rotation around the axis of the surface to obtain, a high density of points depending on how the screen or the surface is rotated. Figure 6(a) shows the image of a screen with spots ordered in a spiral arrangement. The plot of the positions of the centroids for the spots from twelve images captured on each rotation step of the test surface is shown in Fig. 6(b). The screen is designed to increase the density of points with respect to the original radial distribution of the image at the initial position. In Fig. 6(b) a set of equally spaced spots along the radial direction is observed.

One of the main disadvantages of the previous methods, where a movement is applied to the cylindrical screen, is the introduction of errors due to mechanical translation or rotation devices. In a more recent work, the use of LCD flat panels was proposed, for the test of convex surfaces (Moreno-Oliva et al., 2008c); the screens are arranged in a square array and the surface under test is placed in the center. The screens display the required geometry in a sequence so that each distribution of points produces an array of equally spaced spots in the image plane, and the sequence causes these points to move. By taking a picture for each step and merging the centroids of the spot images is possible have a greater density of equidistant spots for better evaluation.

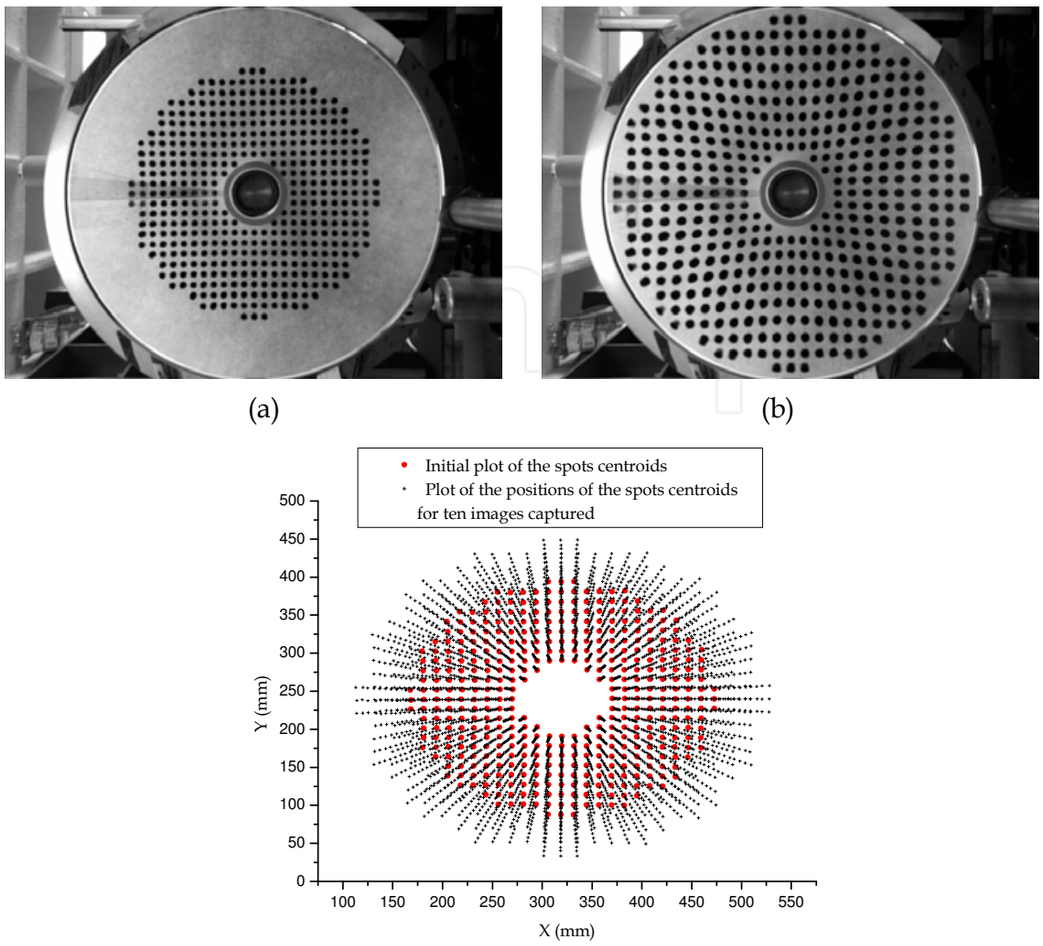

(a) (b) (c)

Fig. 5. a) Image of the screen at the initial position, b) Image of the screen at the final position, c) Plot of the centroid positions of the spots for ten images captured by using the point shifting method.

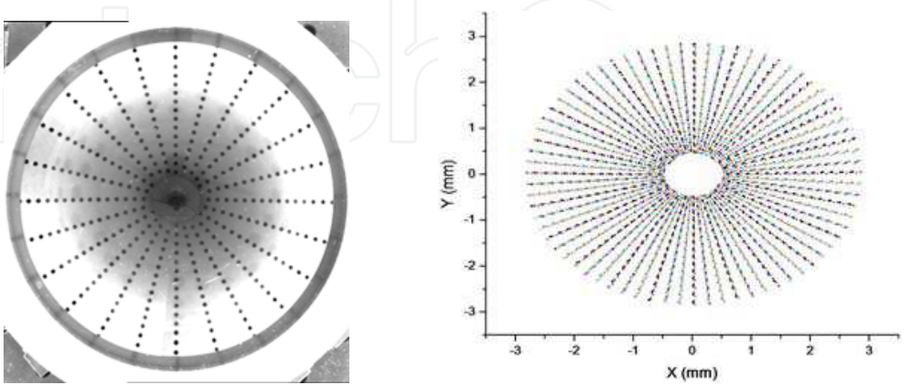

(a) (b)

Fig. 6. a) Image of the screen at the initial position, b) Plot of the position of the centroids for the spots at each rotation step of the test surface.

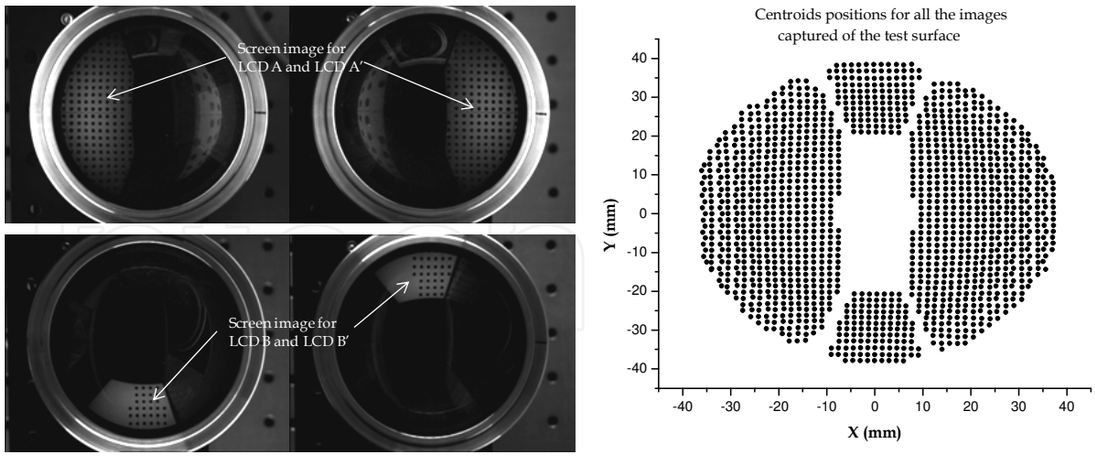

(a) (b)

Fig. 7. (a) Image of each LCD monitor showing a sequence of flat null screens and (b) plot for many sequences of all the LCD monitors.

The screen in this method consisted of four LCD flat panels (LCD A, A' and LCD B, B'), the distance between LCD A and A' is smaller than the distance between LCD B and B', for this reason the image area covered by LCD A and A is greater than that covered by LCD B and B (Fig. 7a). Each LCD displayed a sequence of dynamic flat null screens, and the number of sequences can be increased to the density of equidistant spots. Figure 7b shows the plot of the centroids for all the screens displayed.

3. Testing a parabolic trough solar collector (PTSC)

3.1. Testing a PTSC by area

3.1.1 Screen design

The null screen method can also be used for testing other surfaces without symmetry of revolution such as off-axis parabolic surfaces (Avendaño-Alejo, et al., 2009). This method has also been used in the testing of parabolic trough solar collectors (PTSC). In both cases the use of flat null screens was proposed; the screen is designed in the same way as the cylindrical screens described above, using inverse ray tracing starting on the array of points in the image plane and intercepting the reflected ray on the surface with the flat screen.

The proposal is to use two flat null screens parallel to the collector trough; physically, they are located on each side of a wood or plastic sheet; each side is useful for testing half of the surface of the PTSC. Figure 8 shows the schematic arrangement for the proposed evaluation for a PTSC with flat null screens.

The design of the screen starts on a CCD point P_1, with coordinates $(x,y,a+b)$; the ray passes through the point $P(0,0,b)$ (pinhole of the camera optical system), and arrives at the test surface at $P_2(X,Y,Z)$; after reflection, the ray hits the point $P_3(x_3,y_3,z_3)$ on the null screen (see Fig. 8).

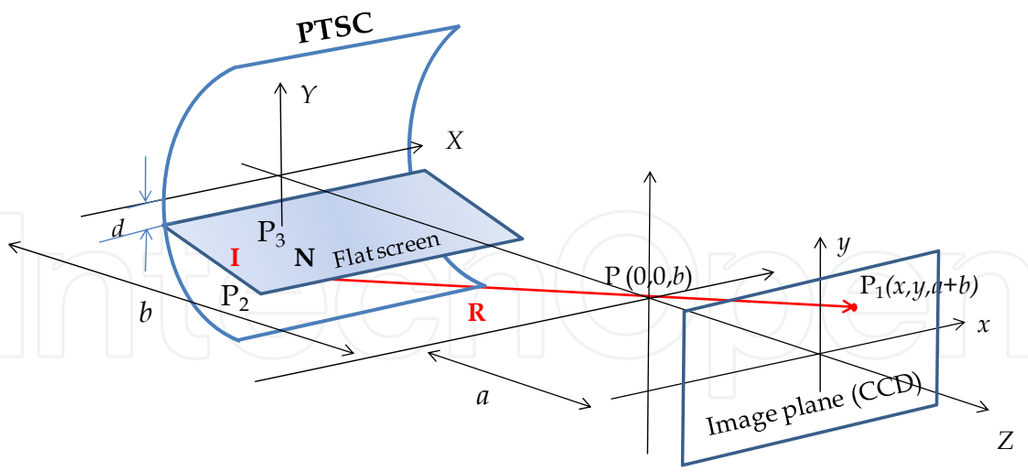

Fig. 8. Setup for the testing for a PTSC with null screens.

The equation for the PTSC is given by.

$$Z = \frac{Y^2}{2r}, \tag{8}$$

where r is the radius of curvature at the vertex. Then, the coordinates of the point P_2 are found by

$$X = tx, \tag{9}$$

$$Y = ty, \tag{10}$$

$$Z = at + b = \frac{Y^2}{2r}, \tag{11}$$

where

$$t = \frac{1}{y^2}\left(ar \pm \sqrt{a^2r^2 + 2y^2rb}\right). \tag{12}$$

Here, a is the distance from the aperture stop to the CCD plane and b is the distance from the aperture stop to the vertex of the surface. Then, using the Reflection Law written as

$$\mathbf{I} = \mathbf{R} - 2(\mathbf{R} - \mathbf{N}) \cdot \mathbf{N}, \tag{13}$$

where **I**, **R**, and **N,** are the incident, reflected and normal unit vectors associate with each corresponding ray. As we are performing an inverse ray trace, the real incident ray is the reflected ray of our tracing. Then, as the normal vector (not normalized) is given by

$$\mathbf{N} = \left(0, \frac{Y}{r}, -1\right), \tag{14}$$

the normalized Cartesian components of the vector **I** are given by

$$\mathrm{I}_x = \frac{x}{\sqrt{x^2+y^2+a^2}}, \quad \mathrm{I}_y = \frac{y(r^2-Y^2)+2arY}{(Y^2+r^2)\sqrt{x^2+y^2+a^2}} \text{ , and } \mathrm{I}_z = \frac{2ryY-a(r^2-Y^2)}{(Y^2+r^2)\sqrt{x^2+y^2+a^2}} \tag{15}$$

Finally, the intersection with the flat null screen gives the coordinates of the point P_3

$$x_3 = tx + s\frac{x}{\sqrt{x^2+y^2+a^2}}, \tag{16}$$

$$y_3 = ty + s\frac{y(r^2-Y^2)+2arY}{(Y^2+r^2)\sqrt{x^2+y^2+a^2}}, \tag{17}$$

$$z_3 = at + b + s\frac{2ryY-a(r^2-Y^2)}{(Y^2+r^2)\sqrt{x^2+y^2+a^2}}, \tag{18}$$

where s is a parameter determined by the condition that the point P_3 is on the flat screen. The equation for this condition is

$$y_3 = d, \tag{19}$$

where d is the distance between the XZ plane and the flat null screen. Substituting Eq. (19) in Eq. (17) yields

$$d = ty + s\frac{y(r^2-Y^2)+2arY}{(Y^2+r^2)\sqrt{x^2+y^2+a^2}}, \tag{20}$$

and solving for s, we get

$$s = \left[\frac{(Y^2+r^2)\sqrt{x^2+y^2+a^2}}{y(r^2-Y^2)+2arY}\right](d-ty). \tag{21}$$

To test the whole area of the PTSC with only one image, it is necessary use two flat null screens in the positions d and $-d$ with respect to the Y axis.

3.1.2 Quantitative surface testing

With the aim of testing a PTSC with the parameter data given in table 2, a null screen was designed. The test surface and the screen designed for it are shown in Fig. 9; the resultant image of the screen after reflection on the test surface is also shown.

Parameter	Symbol	Size
Full aperture	ΔY	3.0 m
Length	L	1.2 m
Focal Length	f	1.0 m
Vertex radius of curvature	r	2.0 m
Stop aperture-CCD plane	a	12.5 mm
CCD length	d	8.1 mm
Stop aperture-surface vertex	b	5192.12 mm

Table 2. Design parameters for the test of a PTSC

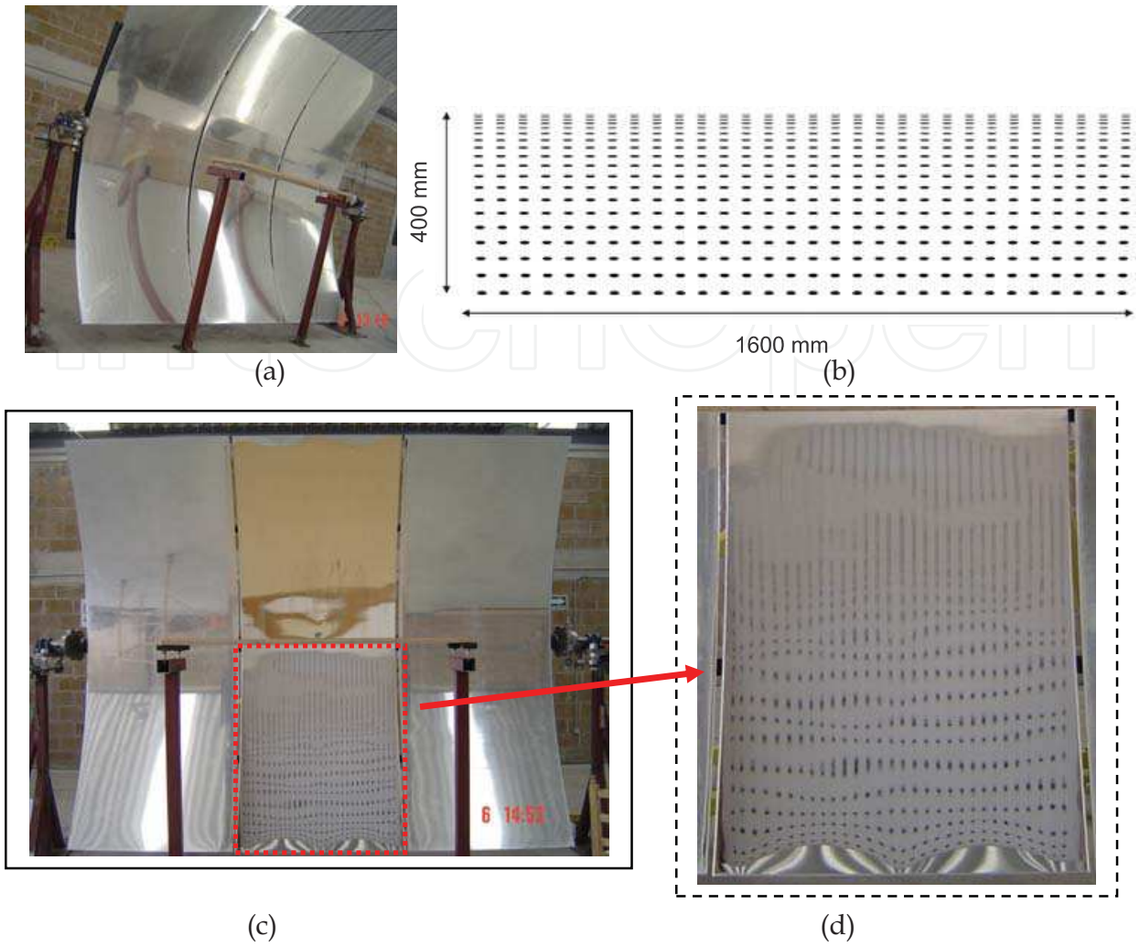

Fig. 9. a) PTSC component, b) flat printed null screen with drop shaped spots for quantitative testing (400x1600 mm), c) image of the screen after reflection on the test area surface, and d) detail of the image.

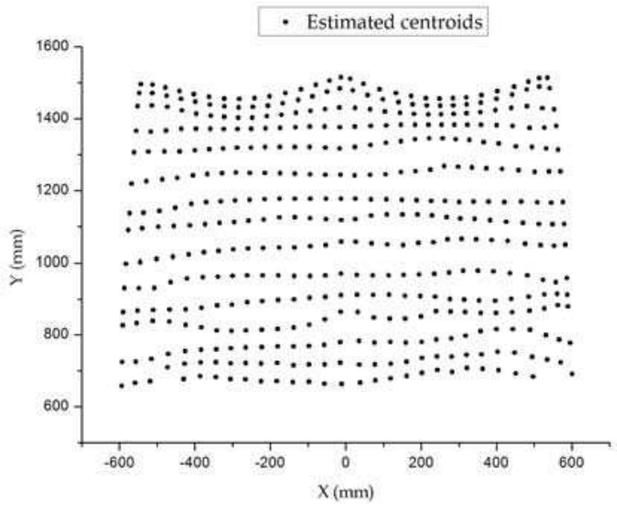

Fig. 10. Plot of the centroid positions for some spots of the flat null screen.

In Fig. 9 the PTSC before assembly is shown, for final assembly it is possible to use a flat null screen for alignment of the PTSC sections. In this example only the result of the test of the lower central panel of the PTSC component is shown. In the qualitative result for the test of a central panel (Fig. 9c) it can clearly be observed that, in general the image shows deformations near the edge of the surface; in the upper part of the image (Fig. 9d) it can be observed that there are doubled or elongated spots. This behavior is due to some small deformations of the test surface. In this case it is not possible to separate the doubled spot images and the surface cannot be tested in this zone, the only spots for which its positions can be determined on the CCD plane (centroids) are show in Fig. 10.
The proposed flat null screen consists of 600 spots, and only 443 were processed for quantitative evaluation.
Having the information of the positions of the centroids on the CCD plane, the normals to the surface are evaluated and the shape of the surface is obtained by using Eq. (3). The method used for the discrete evaluation was the trapezoidal method, which can be written as

$$z_m = -\sum_{i=1}^{m-1}\left\{\left(\frac{n_{x_i}}{n_{z_i}}+\frac{n_{x_{i+1}}}{n_{z_{i+1}}}\right)\frac{(x_{i+1}-x_i)}{2}+\left(\frac{n_{y_i}}{n_{z_i}}+\frac{n_{y_{i+1}}}{n_{z_{i+1}}}\right)\frac{(y_{i+1}-y_i)}{2}\right\}+z_1\,, \tag{22}$$

Here m represents the number of points along some integration path; z_1 is the value for the initial point, which represents only a rigid translation of the surface so it can be approximated by Eq. (11).

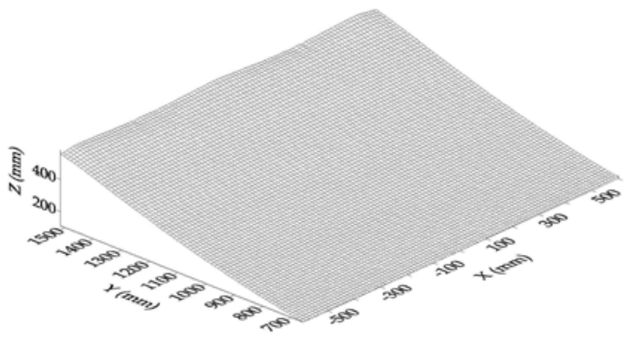

(a)

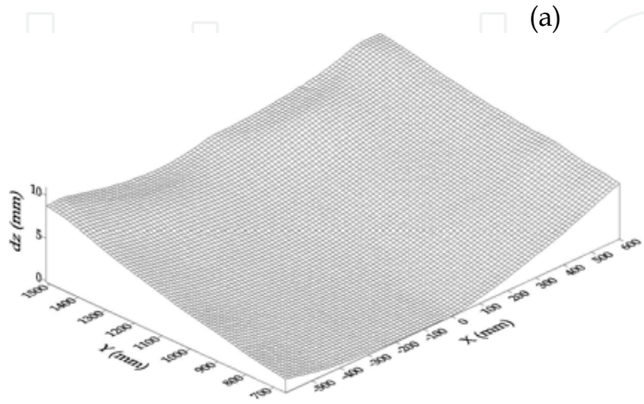

(b)

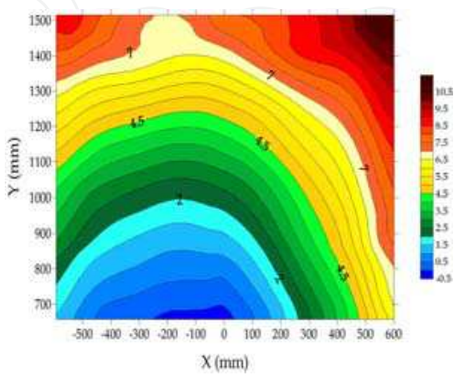

(c)

Fig. 11. a) Evaluated surface, b) Differences in sagitta between the measured surface and the best fit, and c) Contour map of differences in sagitta.

Figure 11a shows the evaluated surface (lower central panel of PTSC); Fig. 11b shows the differences in sagitta (z coordinate) between the evaluated surface and the best fit. In this case the P-V difference in sagitta between the evaluated points and the best fit was $\Delta z_{p\text{-}v}$ = 11.08 mm and the rms difference in the sagitta was Δz_{rms} = 4.89 mm.

3.2 Testing a PTSC by profile

An alternative method for testing the PTSC is given by (Moreno-Oliva et al., 2009); here the test is made by testing one profile at a time with two flat null screens and by scanning the PTSC. All the calculations were made in a meridional plane (X, Y), and for simplicity in the calculus we use an approximation using ellipses instead of drop shaped spots (Carmona-Paredes & Díaz-Uribe, 2007).

A ray starting at point P_1 (α, a +b) on the image plane passes through the pinhole located on the Y axis at a distance b, P (0, b) (Fig. 12), away from the vertex of the surface; this ray arrives at the test surface at the point P_2 (x_2, y_2). After reflection on the PTSC the ray hits the surface at the point P_3 (x_3, y_3) on the flat null screen.

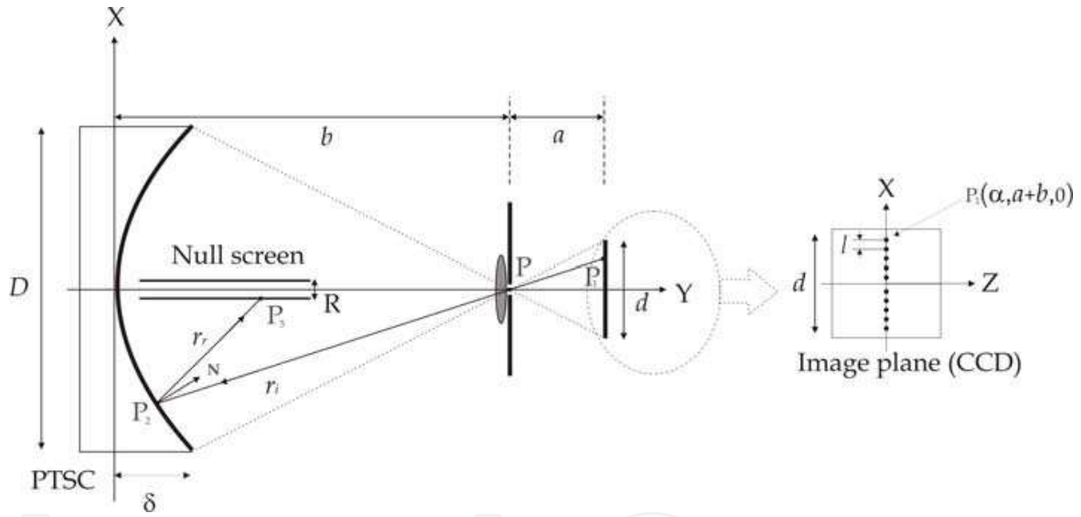

Fig. 12. Layout of the test configuration.

The equation of a parabolic profile with vertex in the origin and axis parallel to the Y axis is

$$y_2 = \frac{x_2^2}{4p}, \tag{23}$$

where p is the focal length of the parabola.

The coordinates of the points that describe the parabolic profile $P_2(x_2, y_2)$, in terms of the parameters of the optical system and the focal length of the parabola p are

$$x_2 = \frac{2pa - 2\sqrt{p^2a^2 + pba^2}}{a}, \tag{24}$$

and the intersection points on the flat null screen $P_3(x_3, y_3)$ are given by

$$y_3 = y - \left[\frac{4ap^2 - 4pxa - x^2a}{x^2a - 2apx - 4pa - 2pxa} \right](x - x_3) , \tag{25}$$

where $x_3 = \mathbf{R}/2$ is constant, **R** is the separation between the flat null screens.
In the meridional plane, with the inverse ray tracing it is only possible to obtain the coordinates of the spots from their center and the vertices along the direction parallel to the Y-axis of each spot in the CCD plane. For each spot on the CCD we obtained three points on the flat null screen (Fig. 13), and according to reference (Carmona-Paredes & Díaz-Uribe, 2007) we can use an approximation using ellipses instead of the drop shape for simplicity in the calculations.

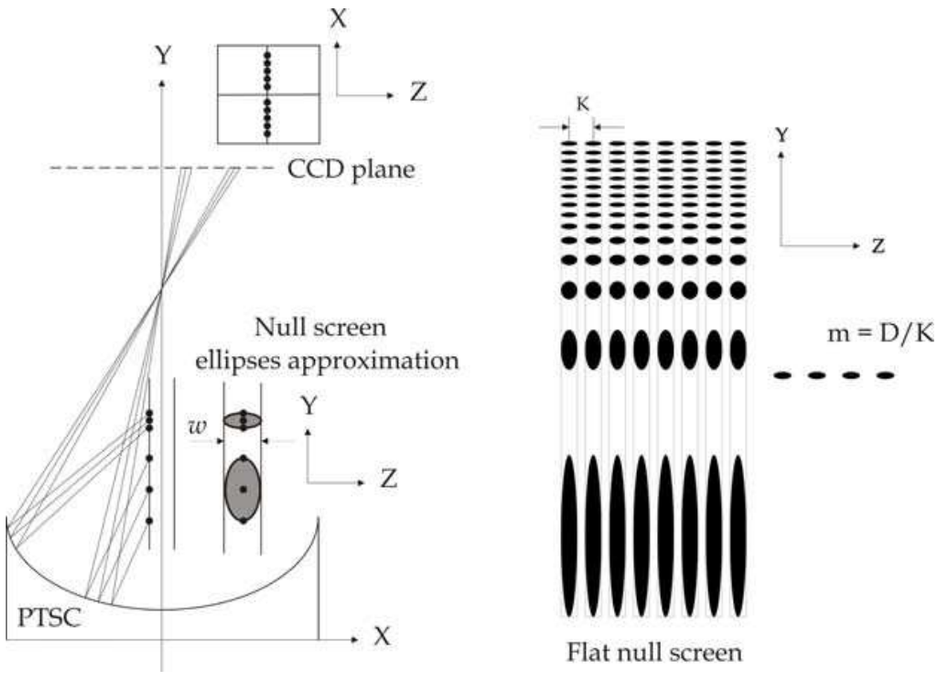

Fig. 13 Inverse ray tracing on the X-Y plane, the elliptical approximation in the Y-Z screen plane, and the flat null screen for testing the PTSC component.

To test the PTSC, the optical system was displaced a distance K and an image for each profile of the PTSC was captured, the PTSC was scanned along the trough (axis Z), m was the number of linear arrangements of spots of the flat null screen, and D the trough length.

4. Testing parabolic dish solar collector systems

In reference (Campos-Garcia et al., 2008) the procedure to obtain the shape of fast concave surfaces is described for a general conic. The same method can be applied to testing of parabolic dish solar collector systems and the equations are simplified if, instead of using a general conic only a parabolic surface is considered. The layout of the test configuration is similar to that of Fig. 1b, starting with one of the points of the proposed arrangement at the

CCD plane $P_1(\rho_1, \phi, a + b)$, where P_1 is given in cylindrical coordinates ($\rho_1 > 0$; $0 \le \phi \le 2\pi$; a, $b > 0$), and the calculations are made for a conic with constant $k = -1$; a ray passing through the point P(0,0,b) (the pinhole of the camera optical system) reaches the surface at the point $P_2(\rho_2, \phi + \pi, z_2)$, where

$$\rho_2 = \frac{ar - \left[a^2 r^2 - 2r\rho_1^2 b\right]^{1/2}}{\rho_1}, \tag{26}$$

$$z_2 = \frac{\rho_2}{\rho_1} a + b, \tag{27}$$

here $r = 1/c$ is the radius of curvature at the vertex, a is the distance from the aperture stop to the CCD plane, and b is the distance from the aperture to the vertex of the surface.
After reflection on the surface the ray hits the cylindrical screen at P_3 (ρ_3, $\phi + \pi$, z_3), where

$$\rho_3 = R, \tag{28}$$

$$z_3 = \frac{-a\rho_2^2 + ar^2 - 2r\rho_1\rho_2}{\rho_1\rho_2^2 - \rho_1 r^2 - 2r\rho_2 a}(-R - \rho_2) + z_2, \tag{29}$$

R is the radius of the cylindrical screen. Distances a and b are chosen in such a way that the image of the whole surface fits the CCD area; they are related by Eq. (1), where D is the diameter of the test surface and β is the sagitta at the rim of the surface, which for a parabolic surface is given by Eq. (2). The method for the surface shape evaluation is as given in section 3.1

5. Conclusion

This Chapter gives a general view of the latest developments of the null screen method and its application in the measurement of the shape of solar collectors. The null screen principles principle has many advantages when compared to other methods; the method does not require a special optical system and its implementation is not very expensive, it is also possible to apply the method to any collector system geometry. With new developments in null screen methods (section 3) it is possible to increase the precision and sensitivity of the quantitative evaluation.

6. References

Avendaño-Alejo, M., Moreno-Oliva, V.I., Campos-García, M. & Díaz-Uribe, R. (2009), Quantitative evaluation of an off-axis parabolic mirror by using a tilted null screen. *Applied Optics*. 48, 1008-1015.

Campos-García, M., Díaz-Uribe, R. & Granados-Agustín, F. (2004). Testing fast aspheric surfaces with a linear array of sources. *Applied Optics*. 43, 6255-6264.

Campos-García M., Díaz-Uribe R. (2008), Quantitative shape evaluation of fast aspherics with null screens by fitting two local second degree polynomials to the surface normals, AIP Conf. Proc. 992, 904-909.

Campos-García, M., Diaz-Uribe, R., & Bolado-Gómez, R. (2008). Testing fast aspheric concave surfaces with a cylindrical null screen. *Applied Optics*. 47, 6, (February 2008) 849-859.

Cordero-Dávila, A., & González-García, J., Surface evaluation with Ronchi test by using Malacara formula, genetic algorithms and cubic splines, in International Optical Design Conference (IODC)/Optical Fabrication and Testing (OF&T) Technical Digest on CD-ROM (Optical Society of America, Washington, DC, 2010), JMB46.

Cornejo-Rodríguez, A. (2007). Ronchi Test, In: *Optical Shop Testing*, D. Malacara, (Wiley, New York), pp. 317-360.

Diaz-Uribe, R., & Campos-García, M. (2000). Null-screen testing of fast convex aspheric surfaces. *Applied Optics*. 39, 16, (June 2000) 2670-2677.

Díaz-Uribe, R. (2000). Medium precision null screen testing of off-axis parabolic mirrors for segmented primary telescope optics; the case of the Large Millimetric Telescope. *Applied. Optics*. 39, 2790-2804.

Díaz-Uribe, R., Granados-Agustín, F., & Cornejo-Rodríguez, A. (2009) "Classical Hartmann test with scanning", Opt. Express, 17, 13959-13973.

Mahajan, V. N., ZernikePolynomials and Wavefront Fitting, In: *Optical Shop Testing*, D. Malacara, 3rd. Ed. (Wiley, New York), pp. 498-546.

Malacara-Doblado, D., & Ghozeil, I. (2007). Hartmann, Hartmann-Shack, and other screen tests, In: *Optical Shop Testing*, D. Malacara, (Wiley, New York), pp. 361-397.

Moreno-Oliva, V.I., Campos-García, M., Bolado-Gómez, R., & Díaz-Uribe, R. (2008a). Point Shifting in the optical testing of fast aspheric concave surfaces by a cylindrical screen. *Applied Optics*. 47, 5, 644-651.

Moreno-Oliva, V.I., Campos-García, M., & Díaz-Uribe, R. (2008b). Improving the quantitative testing of fast aspherics with two-dimensional point shifting by only rotating a cylindrical null screen. *Journal of optics A: Pure and Applied Optics*. 10, 1-7.

Moreno-Oliva, V.I., Campos-García, M., Avendaño-Alejo, M., & Díaz-Uribe, R. (2008c). Dinamic null screens for testing fast aspheric convex surfaces with LCD´s. *Proceedings of 18th IMEKO TC 2 Symposium on Photonics in Measurement*, M. Jedlicka, M. Klima, E. Kostal, P. Pata, eds., (Czech and Slovak Society for Photonics, Czeck Republic, 2008). (1P5, 6pp).

Moreno-Oliva, V.I., Campos-García, M., Granados-Agustín, F., Arjona-Pérez, M.J., Díaz-Uribe & Avendaño-Alejo (2009). Optical testing of a parabolic trough solar collector by null screen with stitching. *Proceedings of SPIE in Modeling Aspects in Optical Metrology II.* edited by Harald Bosse, Bernd Bodermann, Richard M. Silver, Vol. 7390 (October 2009) 739012.

Pottler, K., & Lüpfert, E. (2005). Photogrammetry: A Powerful Tool for Geometric Analysis of Solar Concentrators and Their Components. *Journal of Solar Energy Engineering*. 127, 94-101.

Salas-Peimbert, Malacara-Doblado, Durán-Ramírez, Trujillo-Schiaffino & Malacara-Hernández (2005). Wave-front retrieval from Hartmann test data. *Applied Optics*. 44, 4228-4238.

Shortis M., & Johnston G. (1996). Photogrammetry: An Available Surface Characterization Tool for Solar Concentrators, Part 1: Measurement of Surfaces. *ASME J. of Solar Energy Engineering*, 118,146-150.

IntechOpen

IntechOpen

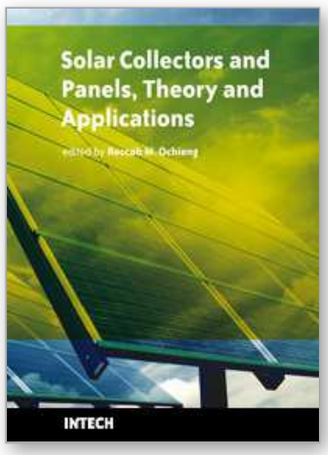

Solar Collectors and Panels, Theory and Applications
Edited by Dr. Reccab Manyala

ISBN 978-953-307-142-8
Hard cover, 444 pages
Publisher Sciyo
Published online 05, October, 2010
Published in print edition October, 2010

This book provides a quick read for experts, researchers as well as novices in the field of solar collectors and panels research, technology, applications, theory and trends in research. It covers the use of solar panels applications in detail, ranging from lighting to use in solar vehicles.

How to reference
In order to correctly reference this scholarly work, feel free to copy and paste the following:

Victor Moreno-Oliva, Rufino Diaz-Uribe and Manuel Campos_García (2010). Shape Measurement of Solar Collectiors by Null Screens, Solar Collectors and Panels, Theory and Applications, Dr. Reccab Manyala (Ed.), ISBN: 978-953-307-142-8, InTech, Available from: http://www.intechopen.com/books/solar-collectors-and-panels--theory-and-applications/shape-measurement-of-solar-collectors-by-null-screens

INTECH
open science | open minds

InTech Europe
University Campus STeP Ri
Slavka Krautzeka 83/A
51000 Rijeka, Croatia
Phone: +385 (51) 770 447
Fax: +385 (51) 686 166
www.intechopen.com

InTech China
Unit 405, Office Block, Hotel Equatorial Shanghai
No.65, Yan An Road (West), Shanghai, 200040, China
中国上海市延安西路65号上海国际贵都大饭店办公楼405单元
Phone: +86-21-62489820
Fax: +86-21-62489821

© 2010 The Author(s). Licensee IntechOpen. This chapter is distributed under the terms of the Creative Commons Attribution-NonCommercial-ShareAlike-3.0 License, which permits use, distribution and reproduction for non-commercial purposes, provided the original is properly cited and derivative works building on this content are distributed under the same license.

IntechOpen

IntechOpen